International Journal of Microwave and Wireless Technologies, 2017, 9(8), 1713–1723.
doi:10.1017/S1759078717000368

RESEARCH PAPER

Perturbation theory-based field analysis of arbitrary-shaped microstrip patch antenna

KARISHMA SHARMA, DHARMENDRA K. UPADHYAY AND HARISH PARTHASARATHY

In this paper, the concept of perturbation theory is applied to derive a general electric field (E-field) expression for any arbitrary-shaped microstrip patch antenna. The arbitrary shape is created by adding small perturbation in a regular patch shape, which is used to find perturbed and unperturbed electromagnetic wave solutions for resultant E-field of patch antenna. Ansoft HFSS simulator is used to validate the derived field expression in curvilinear coordinates for a regular circular-shaped patch. Then the proposed field analysis is applied to develop two new arbitrary-shaped patches in C-band for desired E-field patterns.

Keywords: EM field theory, Antenna design, Modeling and measurements, Perturbation theory

Received 29 December 2016; Revised 16 March 2017; Accepted 22 March 2017; first published online 19 April 2017

I. INTRODUCTION

Microstrip patch antennas (MPA) have been extensively used in wireless communication systems owing to its attractive characteristics, such as low profile, light weight, and ease of fabrication [1]. These antennas consist of a metallic radiating patch on the grounded dielectric substrate with proper feeding techniques as coaxial probe, microstrip line, aperture coupling, and proximity coupling [2–6]. Further, the full-wave analysis is applied to characterize regular shaped patch resonators using the numerical techniques such as mixed potential integral equation (MPIE), finite-difference time-domain (FDTD), finite-element method (FEM) [7–9], etc. Thereafter, modification in the shape of radiating patch has shown to improve the radiation characteristics such as impedance bandwidth, gain, and cross-polarization level (CPL) [10–15]. These modification approaches include, removing or protruding patch metallization [16–20], changing antenna profile through global optimization [21–23], etc. The optimization capabilities of Ansoft HFSS are discussed in [21], which are useful to improve the design within a restricted domain by exploiting the macro scripting language. Later in [22], optimized profiles are obtained for monopole antennas by using global optimization and FEM for ultrawide-band (UWB) applications. Further Tseng and Han [23] applied the CAD-based computation method to achieve an optimum design of broadband, circularly polarized slot antenna.

Furthermore, the numerical analysis has extended to compute various parameters as electric current distribution, input impedance, resonant frequencies, and field patterns for arbitrary-shaped MPA [24–29]. In [24], an improved segmentation technique is developed to analyze arbitrary-shaped antennas for resonant frequency, input impedance, and radiation patterns. Later, Mosig [25] has applied the MPIE technique in irregular microstrip patch shapes using the method of moments (MoM) with subsectional basis functions for current and charge distribution. Then in [26], an efficient approach to compute resonant frequency, modal current, quality factor, and far-field radiation patterns has been developed by using MPIE formulations in space domain. In [27], the point-matching method is adopted for solving resonant frequency of arbitrary-shaped MPA. Further, Yang and Shafai [28] proposed a nodal-based analysis of arbitrary-shaped micrsotrip antenna, which has subdivided geometry, sharing common nodes with orthogonal current components. These node currents are combined to give total patch current. Later, Okoshi's [30] contour integral (CI) method for arbitrary patch shape has been improved by Omar *et al.* [29] using rapidly convergent discretization of patch perimeter only. This improved method includes fringe field correction with physical radiations.

Generally, the perturbation theory comprises a mathematical tool, which approximates a complicated system in terms of simpler one with known solution. Therefore, arbitrary-shaped patches are formed by perturbing the regular shape, which might improve the radiation characteristics [31–34]. In [31], Sun *et al.* have proposed a fast and accurate approach to compute modal solution for an irregular shape of patch derived from a regular shape. Further, broadband or multi-frequency operation mode in perturbed rectangular patch has been acquired for UMTS application [33, 34] and also analyzed through a spectral domain full-wave formulation and MoM numerical technique [35].

In [36, 37], Sarder has presented the perturbation technique incorporated with Green's function and integral equation eigenvalue theory for the analysis of arbitrary shape

Division of Electronics and Communication Engineering, Netaji Subhas Institute of Technology, Delhi University, Delhi, India. Phone: +91 9818 021 456
Corresponding author:
K. Sharma
Email: krrissh_16@yahoo.co.in

represented in the form of refractive index profile. It is noted that, this technique reduces the scalar wave equation to the eigenvalue analysis of integral equation resulting in a rapid and highly accurate semi-analytical method. In a similar manner, the concept of perturbation may be applied to the field analysis of arbitrary patch profiles of microstrip antennas.

This paper presents a simple, fast and robust technique that evaluates electric field (*E*-field) pattern for any perturbed patch shape of microstrip antenna. One of the merits of this presented technique is that the wave equation need only be solved within the region of perturbation than the entire real space, resulting in fast computation in comparison with the other numerical analysis techniques such as FEM, FDTD [36], etc. An arbitrary patch profile is created via perturbation on an unperturbed profile with a known solution, in the curvilinear coordinate system to solve the Helmholtz wave equation. Eigenvalues associated with this equation helps in determining the *E*-field pattern of created arbitrary-shaped MPA.

The rest of the paper is organized as follows. Section II presents the field analysis of perturbed patch profiles in the curvilinear coordinate system. Section III shows the validation of proposed analysis for a regular circular-shaped patch. This section also shows the comparison of theoretical and simulated *E*-field patterns for created arbitrary-shaped patches, to radiate maximally in the directions of $\phi = -45^{\circ}$ and -180°. One of the created MPAs that radiates at $\phi = -180^{\circ}$ is fabricated to validate the proposed analysis with measured results. In last, the conclusions are given in Section IV.

II. FIELD ANALYSIS OF PERTURBED PATCH PROFILES

Field analysis of regular patch shapes have already been characterized using different numerical techniques as FDTD, MPIE [7, 8], etc. Therefore such analysis is also required for arbitrary patch shapes to generalize their radiation characteristics. It is noted that perturbation theory eases the method of finding an approximate mathematical solution for an arbitrary shape, i.e. formed by perturbing the regular patch shape with known solution. This perturbed shape may thus improve the antenna characteristics. Consequently, this section develops a versatile tool to obtain *E*-field pattern of any arbitrary-radiating patch.

Consider an arbitrary-shaped patch lying in the plane of orthogonal curvilinear coordinate system (q_1, q_2, z), i.e. formed by perturbing the regular circular-shaped patch. A Cartesian coordinate system (x, y, z) can be easily transformed into the curvilinear coordinate system using an analytic function F of a complex variable $\not{z} = x + jy$. This analytic function may be represented in terms of real and imaginary parts as $F(\not{z}) = q = q_1 + jq_2$, where q_1 defines a constant boundary of the patch and q_2 is tangential to this boundary. Let function F be invertible to an analytic function G of complex variable q, in curvilinear coordinates. This function $G(q)$ may define any patch profile in curvilinear coordinate system.

Let the circular-shaped patch be represented as $G(q) = e^q$ in curvilinear coordinate system. Now the perturbation is applied over the considered profile $G(q)$ to create an arbitrary-shaped patch $G_1(q)$, which may be defined as:

$$G_1(q) = e^q\,(1 + \delta X(q)), \tag{1}$$

where $X(q)$ defines the perturbation and δ is used to scale the amount of perturbation. Then the Lame's coefficients H_1 and H_2, which univocally determine the reference coordinate system are calculated for the considered perturbed shape $G_1(q)$ to find the wave solution using (2) and (3).

$$H_1 = \left|\frac{\partial G_1(q)}{\partial q_1}\right|, \tag{2}$$

$$H_2 = \left|\frac{\partial G_1(q)}{\partial q_2}\right|. \tag{3}$$

Consider the perturbation $X(q)$ to be symmetric for degeneracy, to obtain the Lame's coefficients as:

$$H_1 = H_2 = \left|G_1'(q)\right| = |e^q(1 + \delta(X(q) + X'(q))). \tag{4}$$

The two-dimensional (2D) Laplacian operator to solve the wave equation in curvilinear coordinates can be expressed as:

$$\begin{aligned}\nabla^2 &= \frac{1}{H_1 H_2}\left(\frac{\partial}{\partial q_1}\frac{H_2}{H_1}\frac{\partial}{\partial q_1} + \frac{\partial}{\partial q_2}\frac{H_1}{H_2}\frac{\partial}{\partial q_2}\right)\\ &= |G_1'(q)|^{-2}\left(\frac{\partial^2}{\partial q_1^2} + \frac{\partial^2}{\partial q_2^2}\right),\end{aligned} \tag{5}$$

where $|G_1'(q)|^2 = |e^q\,(1 + \delta(X(q) + X'(q)))|^2$.

On further simplification $|G_1'(q)|^2$ may be given by:

$$|G_1'(q)|^2 = e^{2q_1}(1 + 2\delta Re(X(q) + X'(q)) + o(\delta^2)). \tag{6}$$

Consider small amount of perturbation ($\delta \to 0$) for neglecting higher order terms in (6), simplified as:

$$|G_1'(q)|^2 = e^{2q_1}(1 + 2\delta\eta(q)), \tag{7}$$

where $\eta(q) = Re(X(q) + X'(q))$.

Consider a MPA having dielectric substrate of permittivity ϵ, permeability μ and height d with circular-shaped patch of radius a. It is assumed that the top and bottom surfaces of this patch are perfect electric conductors while the sidewalls are perfect magnetic conductors. The patch profile is then perturbed by a small amount to create an arbitrary-shaped patch. In general, field configuration is obtained by solving the Helmholtz wave equation [38, 39], therefore this equation is solved in curvilinear coordinates for the considered perturbed patch antenna as:

$$(\nabla^2 + h^2)\psi(q_1,\ q_2) = 0, \tag{8}$$

where h is the wave number and ψ is the scalar wave function. The Laplacian operator in (8) may be expanded by using (5) and for simplicity of resultant equation $\partial/\partial q_1$ is replaced by ∂_1 and $\partial/\partial q_2$ by ∂_2 as given in (9).

$$(\partial_1^2 + \partial_2^2 + |G_1'(q)|^2 h^2)\psi(q) = 0, \tag{9}$$

https://doi.org/10.1017/S1759078717000368 Published online by Cambridge University Press

$|G_1'(q)|^2$ from (7) is substituted into (9) to give:

$$(\partial_1^2 + \partial_2^2 + h^2 e^{2q_1}(1 + 2\delta\eta(q)))\psi(q) = 0, \tag{10}$$

where $\psi(q)$ and h are the effective scalar wave function and wave number, respectively, expressed as:

$$\psi(q) = \psi_o(q) + \delta\psi_1(q) + o(\delta^2), \tag{11}$$

$$h^2 = h_o^2 + \delta h_1^2 + o(\delta^2). \tag{12}$$

Here, $h_o = h_o[m, n] = \alpha_{m,n}/c$ is the wave number for the original patch shape and h_1 is the wave number for the perturbed circular patch shape, in which $\alpha_{m,n}$ represents the TM mode of the radiated wave in curvilinear coordinate system and c is the velocity of light. Also, $\psi_o(q)$ and $\psi_1(q)$ are the scalar functions of original and perturbed patch shape, respectively.

$\psi(q)$ and h^2 from (11) and (12), are substituted into (10). Then the resultant equation is separated into two parts as perturbed and unperturbed, neglecting the higher order terms. Finally, (10) is converted into the following form:

$$\begin{aligned}(\partial_1^2 + \partial_2^2 + h_o^2 e^{2q_1})\psi_o(q) + \delta((\partial_1^2 + \partial_2^2 + h_o^2 e^{2q_1})\psi_1(q) \\ + (h_1^2 e^{2q_1} + 2h_o^2 e^{2q_1}\eta(q))\psi_o(q)) = 0.\end{aligned} \tag{13}$$

Now this wave equation is solved separately for the perturbed and unperturbed parts. Firstly, consider the unperturbed part of (13) as:

$$[\partial_1^2 + \partial_2^2 + h_o^2 e^{2q_1}]\psi_o(q) = 0. \tag{14}$$

The above equation is transferred to polar coordinates (r, ϕ, z) for finding the wave solution using $e^{q_1} = r$ and $q_2 = \phi$. The resultant equation is given below:

$$\left[\frac{1}{r}\frac{\partial}{\partial r} r \frac{\partial}{\partial r} + \frac{1}{r^2}\frac{\partial^2}{\partial \phi^2} + h_o^2\right] \psi_o(r, \phi) = 0. \tag{15}$$

Equation (15) may be solved by using the method of separation of variables, and the separated form is given below:

$$\psi_o(r, \phi) = R(r).\varphi(\phi). \tag{16}$$

Now the separated form of $\psi_o(r, \phi)$ is substituted into (15), which then reduces to two one-dimensional (1D) differential equations. The resultant equations are solved to give a complete solution for ψ_o as:

$$\psi_o(r, \phi) = c_1 u_{mn}(r, \phi) + c_2 v_{mn}(r, \phi), \tag{17}$$

where c_1, c_2 are the scaling coefficients, u_{mn} and v_{mn} represents the normalized versions of $J_m(\alpha_{mn}\ r/a)\cos(m\phi)$ and $J_m(\alpha_{mn}\ r/a)\sin(m\phi)$, respectively, in which J_m is the mth -order Bessel function. These eigenfunctions are orthogonal with respect to $rdrd\phi$ over $0 \le r \le a$ and $0 \le \phi \le 2\pi$. Now the perturbed part of (13) is considered to find solution for scalar function ψ_1 as:

$$\begin{aligned}[\partial_1^2 + \partial_2^2 + h_o^2 e^{2q_1}]\psi_1(q) + h_1^2 e^{2q_1}\psi_o(q) \\ + 2h_o^2 e^{2q_1}\eta(q)\psi_o(q) = 0.\end{aligned} \tag{18}$$

Convert the above equation in polar coordinates as earlier:

$$\begin{aligned}\left[\frac{1}{r}\frac{\partial}{\partial r} r \frac{\partial}{\partial r} + \frac{1}{r^2}\frac{\partial^2}{\partial \phi^2} + h_o^2\right]\psi_1(r, \phi) + h_1^2\psi_o(r, \phi) \\ + 2h_o^2\eta(r, \theta)\psi_o(r, \theta) = 0.\end{aligned} \tag{19}$$

Solution of $\psi_o(r, \theta)$ from (17) is substituted in the above equation, and then the resultant equation is written in Laplacian form as:

$$\begin{aligned}(\nabla^2 + h_o^2[m, n])\psi_1(r, \phi) + h_1^2(c_1 u_{mn} + c_2 v_{mn}) \\ + 2h_o^2[m, n]\eta(r, \phi)(c_1 u_{mn} + c_2 v_{mn}) = 0,\end{aligned} \tag{20}$$

taking inner product with u_{kl} and v_{kl} of the above equation, resulting in (21) and (22).

$$\begin{aligned}(h_o^2[m, n] - h_o^2[k, l])\langle u_{kl},\ \psi_1\rangle + h_1^2(c_1\delta_{mn}.\delta_{ln}) \\ + 2h_o^2[m, n](c_1\langle u_{kl},\ \eta u_{mn}\rangle) + c_2\langle u_{kl}, \eta v_{mn}\rangle) = 0,\end{aligned} \tag{21}$$

$$\begin{aligned}(h_o^2[m, n] - h_o^2[k, l])\langle v_{kl},\ \psi_1\rangle + h_1^2(c_2\delta_{mn}.\delta_{kl}) \\ + 2h_o^2[m, n](c_1\langle v_{kl}, \eta u_{mn}\rangle + c_2\langle v_{kl}, \eta v_{mn}\rangle) = 0.\end{aligned} \tag{22}$$

Rewrite equations (21) and (22) in matrix form for $k = m$ and $l = n$.

$$\begin{bmatrix} 2\beta u_{mn},\ \eta u_{mn} + h_1^2 & 2u_{mn},\ \eta u_{mn}\beta \\ 2\beta v_{mn},\ \eta v_{mn} & 2\beta v_{mn},\ \eta v_{mn} + h_1^2 \end{bmatrix} \begin{bmatrix} c_1 \\ c_2 \end{bmatrix} = 0, \tag{23}$$

where $\beta = h_o^2[m, n]$.

After solving this secular matrix, two perturbed mode eigenvalues for h_1^2 are obtained as $h_{11}^2[m, n]$ and $h_{12}^2[m, n]$, whose corresponding eigenvectors are given below:

$$\begin{bmatrix} c_{11}[m, n] \\ c_{21}[m, n] \end{bmatrix} \quad \text{and} \quad \begin{bmatrix} c_{12}[m, n] \\ c_{22}[m, n] \end{bmatrix}. \tag{24}$$

For $k \ne m$ and $l \ne n$, the eigenvectors may be represented as $c_1 = c_{1i}\ [m, n]$ and $c_2 = c_{2i}\ [m, n]$ for $i \in (1, 2)$ to give the wave solutions for perturbed part as:

$$\langle u_{kl}, \psi_1\rangle = \frac{2h_o^2[m, n](c_{1i}[m, n]\langle u_{kl}, \eta u_{mn}\rangle + c_{2i}[m, n]\langle u_{kl}, \eta u_{mn}\rangle)}{(h_o^2[k, l] - h_o^2[m, n])}, \tag{25}$$

$$\langle v_{kl},\ \psi_1\rangle = \frac{\begin{aligned}2h_o^2[m, n](c_{1i}[m, n]\langle v_{kl}, \eta v_{mn}\rangle \\ + c_{2i}[m, n]\langle v_{kl},\ \eta v_{mn}\rangle)\end{aligned}}{(h_o^2[k, l] - h_o^2[m, n])}. \tag{26}$$

The generalized solution for the perturbed part ψ_1 is obtained by combining the solutions in (25) and (26).

$$\psi_{1i}(r, \phi) = \sum_{(k,l) \ne (m,n)} \{u_{kl}(r, \phi)\langle u_{kl}, \psi_{1i}\rangle + v_{kl}(r, \phi)\langle v_{kl}, \psi_{1i}\rangle\}. \tag{27}$$

https://doi.org/10.1017/S1759078717000368 Published online by Cambridge University Press

Now, the resultant solutions for perturbed and unperturbed parts are transformed into curvilinear coordinates. This transformation results as:

$$\psi_o(q_1, q_2) = c_1 u_{mn}(q_1, q_2) + c_2 v_{mn}(q_1, q_2), \tag{28}$$

$$\delta\psi_{1i}(q_1, q_2) = \delta \sum_{(k,l) \neq (m,n)} \{u_{kl}(q_1, q_2)\langle u_{kl}, \psi_{1i}\rangle + v_{kl}(q_1, q_2)\langle v_{kl}, \psi_{1i}\rangle\}. \tag{29}$$

Therefore, E-field in the z-direction for the perturbed radiating patch is given below.

$$\begin{aligned} E_{z_{mni}}(q_1, q_2) &= \psi_o(q_1, q_2) + \delta\psi_{1i}(q_1, q_2) \\ &= c_{1i}[m, n]u_{mn}(q_1, q_2) + c_{2i}[m, n]v_{mn}(q_1, q_2) \\ &\quad + \delta \sum_{(k,l)\neq(m,n)} \left\{ \begin{matrix} u_{kl}(q_1, q_2)\langle u_{kl}, \psi_{1i}\rangle + \\ v_{kl}(q_1, q_2)\langle v_{kl}, \psi_{1i}\rangle \end{matrix} \right\}. \end{aligned} \tag{30}$$

A generalized form of radiating E-field in the z-direction for arbitrary-shaped MPA may be represented as:

$$E_z(q_1, q_2, z) = \sum_{mnpi} E_{z_{mni}}(q_1, q_2) \sin\left(\frac{\pi p z}{d}\right) Re\{Y\}, \tag{31}$$

where m, n, p are the positive integers and $Y = \alpha_{mnpi} e^{(j(h_b^{[m,\ n]2} + \delta h_{1i}[m,\ n]^2 + (\pi^2 p^2/d^2))^{1/2} t)}$, for which α_{mnpi} are complex scalars.

This equation may be used to find E-field pattern for TM_{mn} mode of any arbitrary-shaped patch antenna. Such E-field pattern for any antenna structure may also be obtained by using any commercial software like, FEM-based Ansoft HFSS [40]. However, there is a difference in the way by which these methods are applied on the geometry of the microstrip patch antenna for its field analysis. In the proposed method, the wave equation needs to be solved only within the region of perturbation, and a continuous solution to the potential is obtained in terms of superposition of sine and cosine functions. Also, for better approximation to the true solution higher order perturbation can be applied. Whereas the technique of FEM involves approximation of a continuous potential by discrete vertex potentials in the entire real space, and the grid elements are made smaller for approximating closer to the solution, which increases the overall computation time. This certainly makes the proposed method simpler, accurate and faster in comparison with the FEM-based technique for far-field analysis of arbitrary patch shapes. However, FEM can give more accurate field analysis for patch shapes where there is any change within the boundary such as dissimilar material properties, creation of complex geometry inside the boundary, etc. as this method captures the local regional effects [9].

Section III gives the validation of derived E-field equation by numerically analyzing E-field for various patch shapes of microstrip antenna using MATLAB software, and then simulating these arbitrary radiating patch antennas using Ansoft HFSS software for validation.

III. ANTENNA CONFIGURATION AND RESULTS

The derived E-field expression in the previous section can be obtained by evolving the considered shape $G_1(q)$ in curvilinear coordinate system for which the symmetric perturbation $X(q)$ represented as:

$$X(q) = \sum_{k=1}^{p} c_k q^k, \tag{32}$$

where coefficients c_k are used to define the symmetric perturbation. These coefficients can be varied to obtain a particular patch shape for desirable field pattern. After substitution of $X(q)$ from (32) into (1), the considered shape $G_1(q)$ can be expressed as:

$$G_1(q) = e^q \left(1 + \delta \sum_{k=1}^{p} c_k q^k\right). \tag{33}$$

A regular circular-shaped MPA is considered for validation of E-field expression, i.e. defined in (31). Then the coefficients c_k are varied to form two different arbitrary patch shapes for desired directional field patterns. The following subsections show the comparison of theoretical (MATLAB) and simulated (HFSS) results for all the patch shapes, in which the last

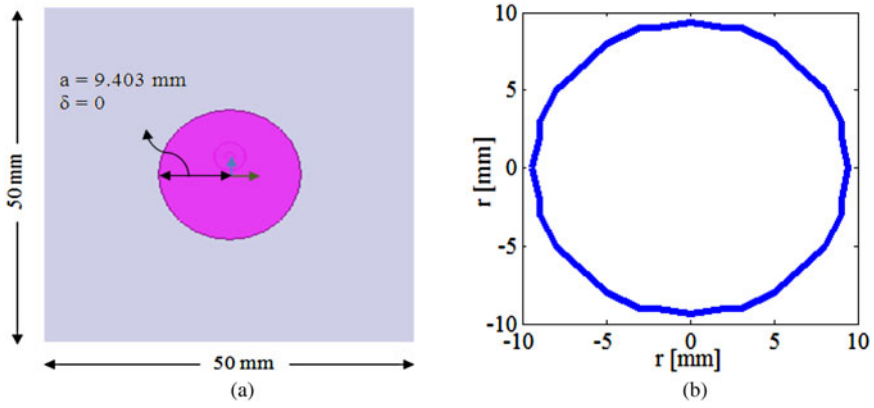

Fig. 1. Circular shape ($\phi = 0^\circ$). (a) Layout of circular-shaped MPA; (b) theoretical unperturbed circular patch shape.

https://doi.org/10.1017/S1759078717000368 Published online by Cambridge University Press

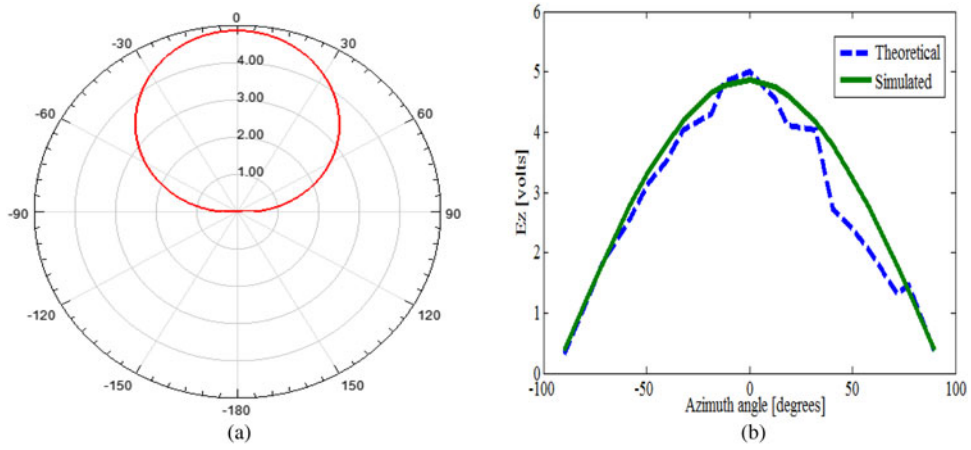

Fig. 2. Radiation patterns for circular-shaped MPA ($\phi = 0^{\circ}$). (a) Simulated *E*-field pattern for $-90^{\circ} < \phi < 90^{\circ}$ (clockwise), (b) comparison of the simulated and theoretical *E*-field patterns for $-90^{\circ} < \phi < 90^{\circ}$ (clockwise).

section also includes the validation of proposed analysis with measured result for one of the created arbitrary patch shapes.

A) Circular patch antenna ($\phi = 0^{\circ}$)

It is noted that C-band has various applications in today's scenario in satellite communication, Wi-Fi devices, weather radar systems etc. and also it offers minimal interference from severe weather conditions resulting in consistent, reliable services for any location. Therefore, this operating band is selected to design a regular circular-shaped MPA to radiate maximally at azimuth angle (*xy*-plane) $\phi = 0^{\circ}$.

As per the conventional design procedure [1], initial dimensions of a circular-shaped MPA are calculated for the

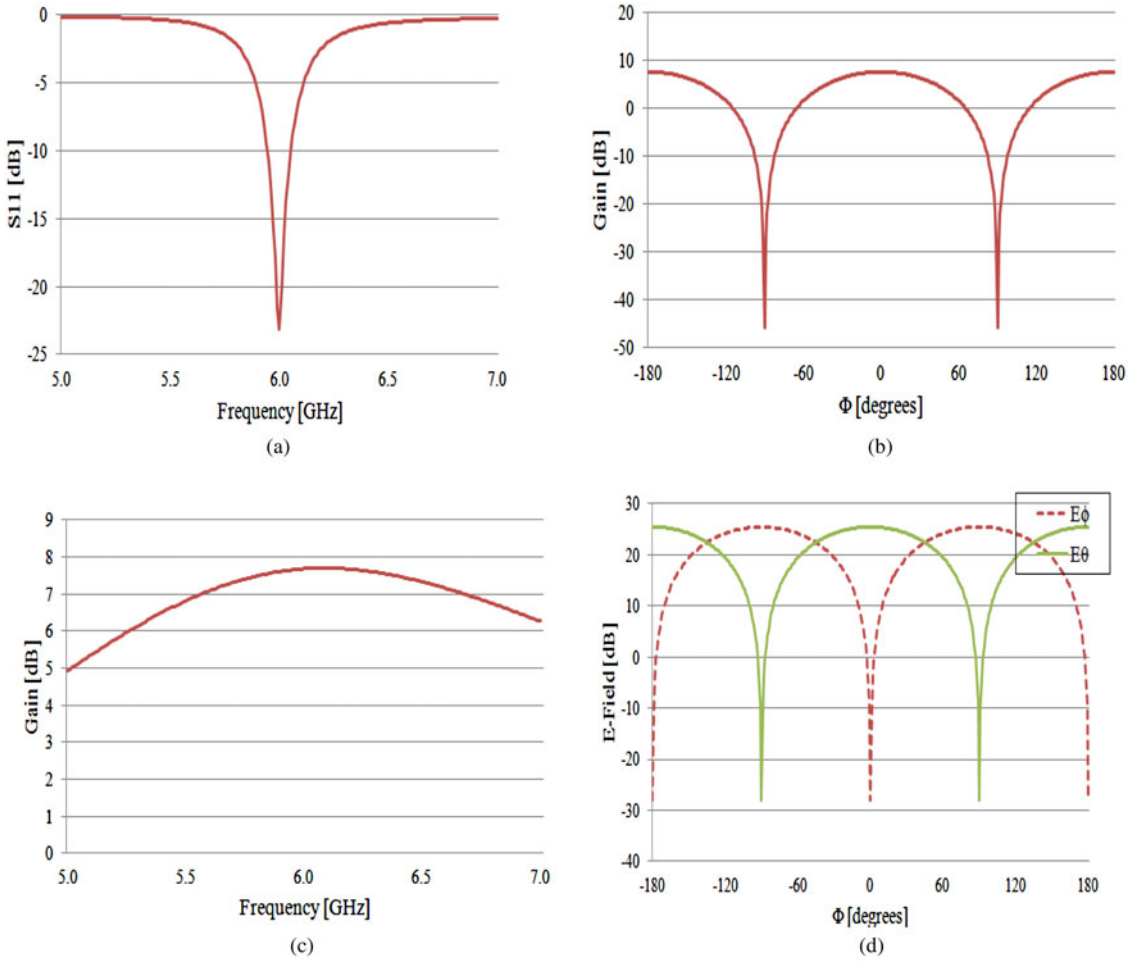

Fig. 3. Characteristics of circular MPA ($\phi = 0^{\circ}$). (a) Return loss, (b) gain versus ϕ, (c) gain versus frequency, (d) cross-polarization level.

https://doi.org/10.1017/S1759078717000368 Published online by Cambridge University Press

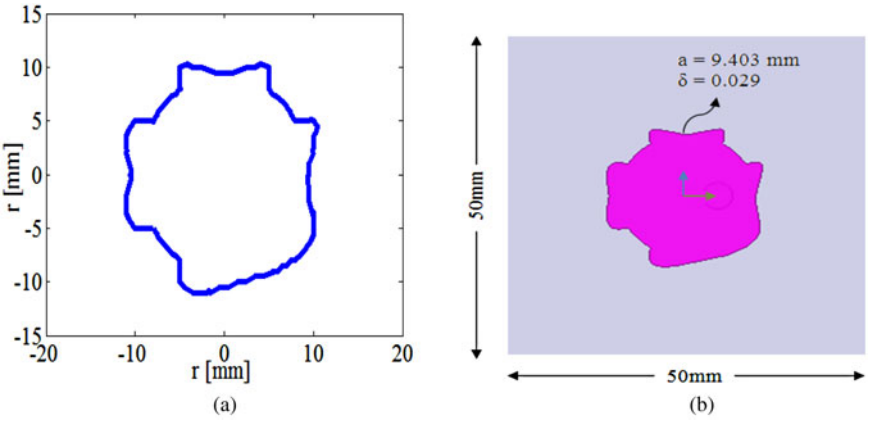

Fig. 4. Arbitrary shape ($\phi = -45^\circ$). (a) Theoretical arbitrary-shaped patch, (b) layout of arbitrary-shaped MPA.

design frequency of 6 GHz. The antenna layout consists of a circular-shaped patch on grounded dielectric substrate RT/Duroid with relative permittivity ϵ_r of 2.2 and thickness of 0.762 mm, having an overall dimension of 50 mm × 50 mm. Initial simulations are performed to obtain the resonant frequency exactly at 6 GHz, which results into the radius of circular patch a =9.403 mm [11]. Coaxial probe feeding technique is used to feed the radiating patch since it has the merit of design simplicity through positioning of feed point to adjust the input impedance level [7]. Simulated E-field pattern is compared with the theoretical pattern for considered unperturbed circular patch shape $G_1(q)$.

Figure 1(a) shows the physical layout of considered circular-shaped MPA and Fig. 1(b) shows the corresponding theoretical shape $G_1(q)$ with the scaling parameter $\delta = 0$. The structure given in Fig. 1(a) is now simulated to obtain the E-field pattern at elevation angle (yz-plane) $\theta = 90^\circ$ for comparison with the theoretical pattern $E_z(q_1, q_2, z)$.

Figure 2(a) shows the simulated E-field pattern for resonant frequency 6 GHz and Fig. 2(b) gives the comparison of the simulated and theoretical E-field patterns. These results signify that the simulated E-field pattern is similar to the theoretical pattern. Further, it is observed that the maximum and minimum strengths of the simulated E-field are 4.85 ($\phi = 0^\circ$) and 0.39 ($\phi = 90^\circ$), respectively; however the theoretical values are 5.01 ($\phi = 0^\circ$) and 0.36 ($\phi = 90^\circ$). These observations validate the theoretical results. It is also noted that the simulated results are broadside symmetric for the considered circular MPA.

Figure 3 shows the other characteristics for circular MPA as return loss, gain versus ϕ, gain versus frequency and CPL. From Fig. 3(a), it is observed that the considered radiating patch resonates at 6 GHz with return loss −23.14 dB, having the impedance bandwidth of 120 MHz. Further, Fig. 3(b) shows the value of broadside gain as 7.68 dB ($\phi = 0^\circ$) at 6 GHz; however Fig. 3(c) gives gain of 7.70 dB ($\phi = 0^\circ$) at 6.09 GHz. The field components E_θ and E_ϕ are also traced at $\theta = 90^\circ$ in Fig. 3(d) to calculate CPL of −53 dB.

B) Arbitrary-shaped antenna ($\phi = -45^\circ$)

The coefficients of the patch shape $G_1(q)$ are varied to perturb the considered circular shape of patch for achieving the desired radiation characteristics. Therefore, a new arbitrary patch shape is evolved, i.e. perturbed at the circumference of circular patch, which has the maximum field strength directed at $\phi = -45^\circ$. Figure 4(a) shows the developed theoretical shape $G_1(q)$ with $\delta = 0.029$ and Fig. 4(b) shows the

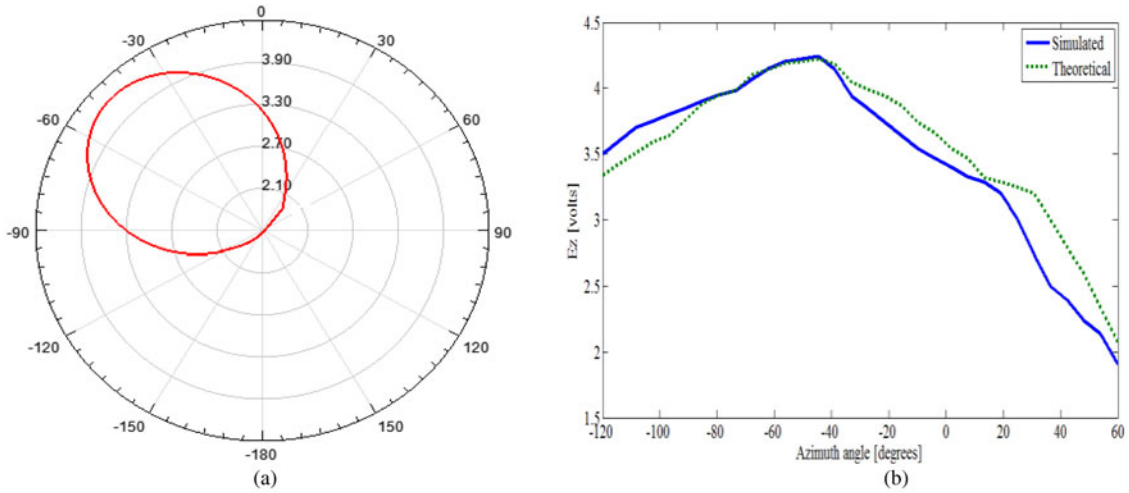

Fig. 5. Radiation patterns for arbitrary-shaped MPA ($\phi = -45^\circ$). (a) Simulated E-field pattern for $-120^\circ < \phi < 60^\circ$ (clockwise), (b) comparison of the theoretical and simulated E-field patterns for $-120^\circ < \phi < 60^\circ$ (clockwise).

https://doi.org/10.1017/S1759078717000368 Published online by Cambridge University Press

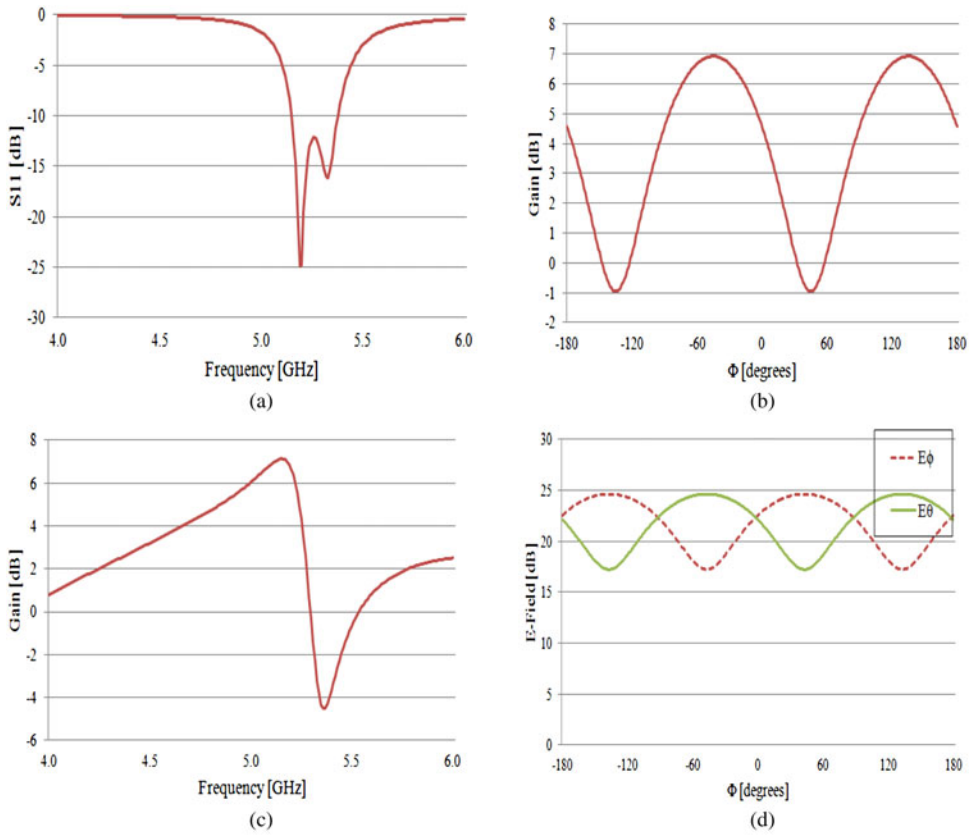

Fig. 6. Characteristics of arbitrary-shaped MPA ($\phi = -45^{\circ}$). (a) Return loss, (b) gain versus ϕ, (c) gain versus frequency, (d) cross-polarization level.

corresponding layout of proposed arbitrary shape ($\phi = -45^{\circ}$), preserving the structure configuration of original circular MPA.

The proposed arbitrary-shaped MPA ($\phi = -45^{\circ}$) is simulated, then it is observed that the resonant frequency shifted to 5.18 GHz owing to change in effective dimensions of considered patch. Figure 5(a) shows the simulated *E*-field pattern ($\theta = 90^{\circ}$) and Fig. 5(b) shows the comparison of theoretical and simulated *E*-field patterns. It clears that the simulated field pattern is comparable with the theoretical pattern. Further, it is observed that the direction of maximum field strength rotates anticlockwise by 45° as compared with that of circular MPA, the maximum strengths of simulated and theoretical *E*-field are 4.24 and 4.22 at $\phi = -45^{\circ}$ respectively, however the minimum strengths are 1.76 ($\phi = 60^{\circ}$) and 1.83 ($\phi = 10^{\circ}$).

Figure 6 shows the other antenna characteristics for arbitrary-shaped MPA ($\phi = -45^{\circ}$) as return loss, gain versus ϕ, gain versus frequency and CPL. Figure 6(a) clears that the considered radiating patch resonates at 5.18 GHz with return loss −24.82 dB, having the improved impedance bandwidth of 230 MHz as compared with that of circular MPA. Further, Fig. 6(b) shows the gain as 6.87 dB ($\phi = -45^{\circ}$) at 5.18 GHz; however Fig. 6(c) gives gain of 7.13 dB ($\phi = -45^{\circ}$) at 5.15 GHz. From Fig. 6(d), it is clear that the CPL is reduced to −7.40 dB. Therefore, the proposed structure has trade-off between the impedance bandwidth and CPL characteristics. Circular polarization is also observed in Fig. 7 for the proposed radiating structure with axial ratio of 0.32 dB at resonant frequency.

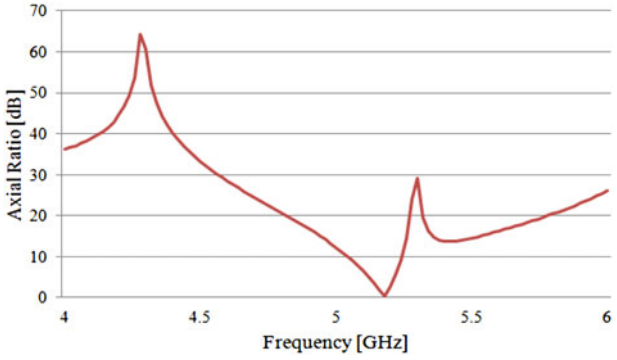

Fig. 7. Axial ratio of arbitrary-shaped MPA ($\phi = -45^{\circ}$).

C) Arbitrary-shaped antenna ($\phi = -180^{\circ}$)

The coefficients for the patch shape $G_1(q)$ are again varied for achieving maximum *E*-field strength along direction $\phi = -180^{\circ}$. This variation perturbs the circular shape to new arbitrary shape with $\delta = 0.052$, i.e. given in Fig. 8(a). Further, Fig. 8(b) shows the corresponding layout of proposed arbitrary shape ($\phi = -180^{\circ}$), preserving the structure configuration of original circular MPA. This shape is also fabricated to validate the proposed technique, i.e. creating arbitrary-shaped MPAs for the desired field pattern, with measured results. The fabricated model is shown in Fig. 8(c).

https://doi.org/10.1017/S1759078717000368 Published online by Cambridge University Press

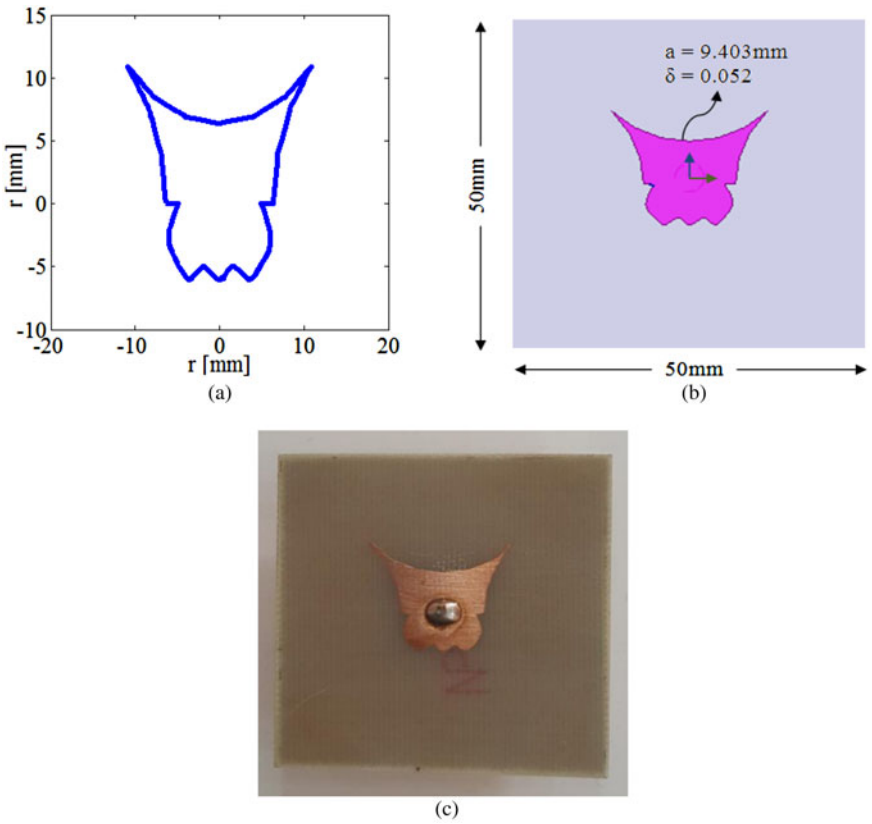

Fig. 8. Arbitrary shape ($\phi = -180^\circ$). (a) Theoretical arbitrary-shaped patch, (b) layout of arbitrary-shaped MPA, (c) prototype of arbitrary-shaped patch antenna.

The proposed arbitrary-shaped MPA ($\phi = -180^\circ$) is simulated, and then it is observed that the resonant frequency shifted to 6.34 GHz due to the variation in effective dimensions of considered patch. Figure 9(a) shows the simulated *E*-field pattern ($\theta = 90^\circ$) and Fig. 9(b) shows the comparison of theoretical, simulated, and measured *E*-field patterns. These radiation results clear that the measured and simulated pattern appears to be same as the theoretical pattern. It is also observed that the direction of maximum field strength rotates anticlockwise by 180° as compared with that of circular MPA. Further, it is noted that the maximum strengths of measured, simulated and theoretical *E*-field are 4.82, 4.96, and 4.87 at $\phi = -180^\circ$; respectively; however, the minimum strengths are 1.48, 0.96, and 1.00 at $\phi = 90^\circ$.

Figure 10 shows the other characteristics for arbitrary-shaped MPA ($\phi = -180^\circ$) as return loss, gain versus ϕ, gain versus frequency and CPL. It is observed from Fig. 10(a) that this patch antenna resonates at 6.34 GHz with return loss −12.16 dB, having the impedance bandwidth of 40 MHz as compared with that of original circular MPA.

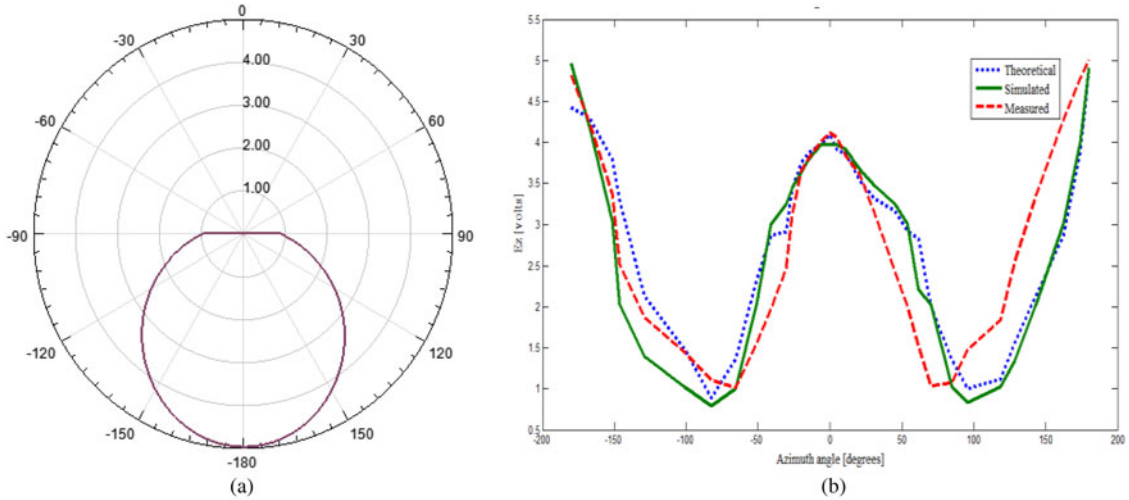

Fig. 9. Radiation patterns for arbitrary-shaped MPA ($\phi = -180^\circ$). (a) Simulated *E*-field pattern for $-90^\circ < \phi < 90^\circ$ (anticlockwise), (b) comparison of theoretical and simulated *E*-field patterns for $-90^\circ < \phi < 90^\circ$ (anticlockwise).

https://doi.org/10.1017/S1759078717000368 Published online by Cambridge University Press

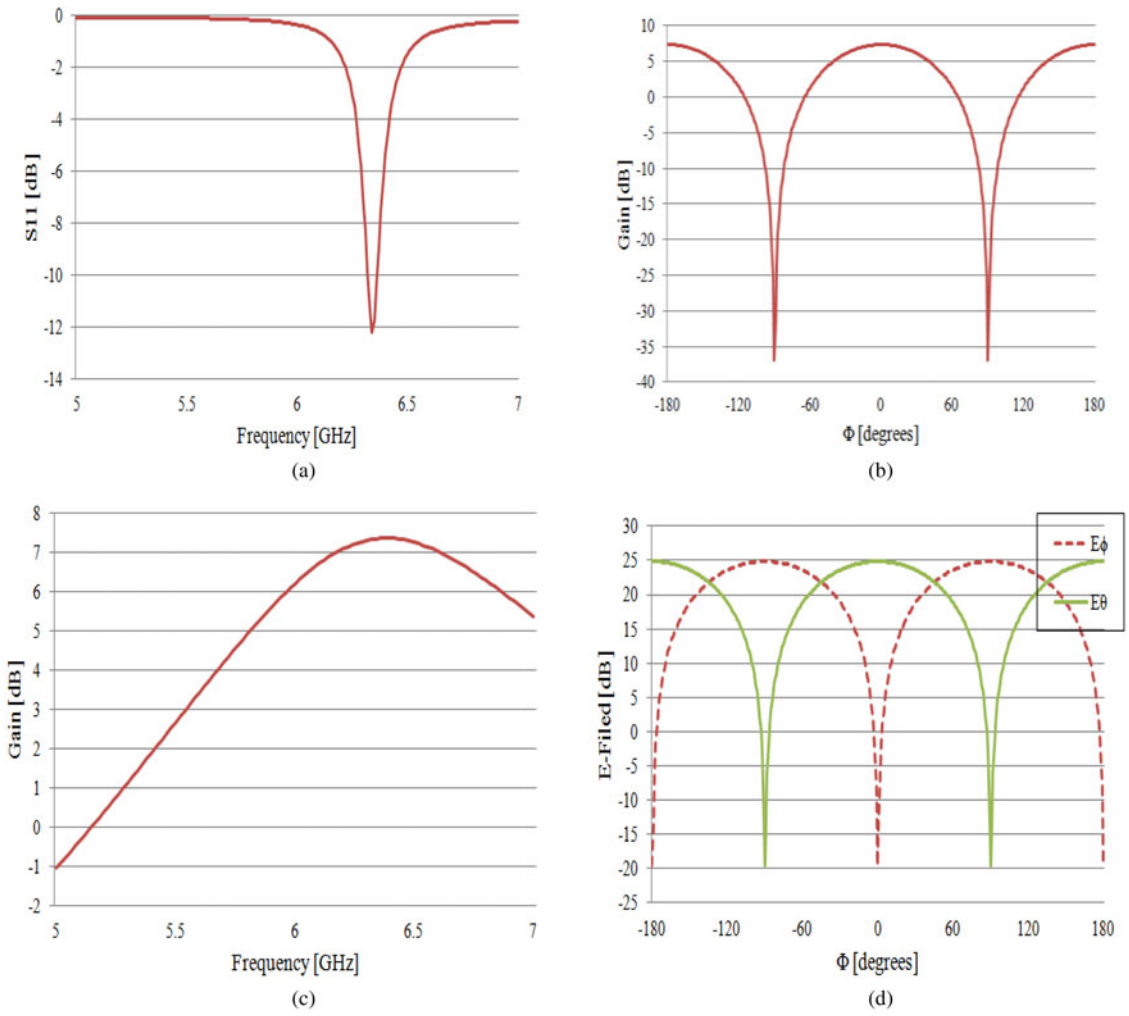

Fig. 10. Characteristics of arbitrary-shaped MPA ($\phi = -180^\circ$). (a) Return loss, (b) gain versus ϕ, (c) gain versus frequency, (d) cross-polarization level.

Further, Fig. 10(b) clears that the gain is 7.36 dB ($\phi = -180^\circ$) at 6.34 GHz; however, Fig. 10(c) gives gain of 7.37 dB ($\phi = -180^\circ$) at 6.35 GHz. Figure 10(d) shows that the CPL is reduced to −44.31 dB. These observations may conclude that the theoretical *E*-field pattern for any patch shape holds in good agreement with the simulated HFSS results.

IV. CONCLUSION

Field analysis of an arbitrary-shaped MPA is evolved by deriving the *E*-field expression based on the concept of perturbation theory. Change in the geometry of a radiating patch varies the impedance and radiation characteristics such as gain, bandwidth, CPL, direction of radiation, etc. A mathematical perturbed shape is defined in the curvilinear coordinate system to create different arbitrary patch shapes for the desired radiation pattern. Initially, a regular circular-shaped MPA is designed for broadside radiation pattern ($\phi = 0^\circ$) to validate the evolved field analysis. Further, this analysis is used to create two arbitrary-shaped patch antennas, which radiate maximally in the directions of $\phi = -45^\circ$ and -180°. The simulated results show that the designed MPA ($\phi = -45^\circ$) has improved bandwidth of 230 MHz with additional characteristic of circular polarization at resonant frequency, and other designed MPA ($\phi = -180^\circ$) radiates exactly in opposite direction to that of circular MPA, preserving its radiation characteristics at the cost of impedance bandwidth. The method presented in this paper is simple, accurate, adaptable, fast, and will serve as a useful tool in the design and analysis of MPA for pattern specific applications.

ACKNOWLEDGEMENTS

The authors are highly grateful to the Director of NSIT, Delhi, India, for his constant encouragement and provision of facilities for this research work. Also, we are thankful to the anonymous reviewers for their constructive comments, which helped us improve the manuscript.

REFERENCES

[1] Balanis, C.A.: Antenna Theory – Analysis and Design, J. Wiley & Sons Inc., New York, 1997.

[2] Garg, R.; Bhartia, P.; Bahl, I.; Ittipiboon, A.: Microstrip Antenna Design Handbook, Artech House, London, 2001.

https://doi.org/10.1017/S1759078717000368 Published online by Cambridge University Press

[3] Carver, K.R.; Mink, J.W.: Microstrip antenna technology. IEEE Trans. Antennas Propag., **29** (1981), 2–24.

[4] Singla, G.; Khanna, R.: Modified CPW-fed rotated E-slot antenna for LTE/WiMAX applications. Int. J. Microw. Wireless Tech., **7** (2015), 535–542.

[5] Tinoco, A.F.; Nascimento, D.C.; Schildberg, R.; Lacava, J.C.Da.S.: Analysis and design of rectangular microstrip antennas for educational purposes. IEEE Antennas Propag. Mag., **53** (2011), 151–155.

[6] Peixeiro, C.: Microstrip antenna papers in the IEEE transactions on antennas and propagation. IEEE Antennas Propag. Mag., **54** (2012), 264–268.

[7] James, J.R.; Hall, P.S.: Handbook of Microstrip Antennas, Peter Peregrinus Ltd., London, 1989.

[8] Schejbal, V.; Novak, J.; Gregora, S.: Comparison of CAD for rectangular microstrip antennas. Radioengineering, **12** (2003), 12–15.

[9] Madenci, E.; Guven, I.: The Finite Element Method and Applications in Engineering Using ANSYS®, Springer, New York, 2015.

[10] Islam, M.T.: Broadband E-H shaped microstrip patch antenna for wireless systems. Prog. Electromagn. Res., **98** (2009), 163–173.

[11] Sharma, K.; Upadhyay, D.K.; Parthasarathy, H.: Modified circular-shaped microstrip patch antenna, in IEEE Int. Conf. on Computational Intelligence & Communication Technology, Ghaziabad (India), 2015, 397–399.

[12] Ang, B.K.; Chung, B.K.: A wideband E-shaped microstrip patch antenna for 5–6 GHz wireless communications. Prog. Electromagn. Res., **79** (2007), 397–407.

[13] Moradikordalivand, A.; Rahman, T.A.: Broadband modified rectangular micro-strip patch antenna using stepped cut at four corners method. Prog. Electromagn. Res., **137** (2013), 599–619.

[14] Le, T.T.; Park, H.C.: Very simple circularly polarised printed patch antenna with enhanced bandwidth. Electron. Lett., **50** (2014), 1896–1898.

[15] Ghosh, A.; Ghosh, S.K.; Ghosh, D.; Chattopadhyay, S.: Improved polarization purity for circular microstrip antenna with defected patch surface. Int. J. Microwave Wireless Tech., **8** (2016), 89–94.

[16] Noghabaei, S.M.; Rahim, S.K.A.; Soh, P.J.; Vandenbosch, G.A.E.: A dual-band circularly-polarized patch antenna with a novel asymmetric slot for WiMAX application. Radioengineering, **22** (2013), 291–295.

[17] Gautam, A.K.; Kunwar, A.; Kanaujia, B.K.: Circularly polarized arrowhead-shaped slotted microstrip antenna. IEEE Antennas Wireless Propag. Lett., **13** (2014), 471–474.

[18] Sharma, V.; Sharma, M.M.: Dual band circularly polarized modified rectangular patch antenna for wireless communication. Radioengineering, **23** (2014), 195–202.

[19] Khan, M.U.; Sharawi, M.S.; Mittra, R.: Microstrip patch antenna miniaturisation techniques: a review. IET Microw. Antennas Propag., **9** (2015), 913–922.

[20] Farswan, A.; Gautam, A.K.; Kanaujia, B.K.; Rambabu, K.: Design of Koch fractal circularly polarized antenna for handheld UHF RFID reader applications. IEEE Trans. Antennas Propag., **64** (2016), 771–775.

[21] Ansoft Corp.: Parametrics and optimization using Ansoft HFSS. Microw. J. – Euro. Glob. Ed., **42** (1999), 156–167.

[22] Martinez-Fernandez, J.; Gil, J.M.; Zapata, J.: Ultrawideband optimized profile monopole antenna by means of simulated annealing algorithm and the finite element method. IEEE Trans. Antennas Propag., **55** (2007), 1826–1832.

[23] Tseng, L.-Y.; Han, T.-Y.: An evolutionary design method using genetic local search algorithm to obtain broad/dual-band characteristics for circular polarization slot antennas. IEEE Trans. Antennas Propag., **58** (2010), 1449–1456.

[24] Palanisamy, V.; Garg, R.: Analysis of arbitrarily shaped microstrip patch antennas using segmentation technique and cavity model. IEEE Trans. Antennas Propag., **34** (1986), 1208–1213.

[25] Mosig, J.R.: Arbitrarily shaped microstrip structures and their analysis with a mixed potential integral equation. IEEE Trans. Microw. Theory Tech., **36** (1988), 314–323.

[26] Michalski, K.A.; Zheng, D.: Analysis of microstrip resonators of arbitrary shape. IEEE Trans. Microw. Theory Tech., **40** (1992), 112–119.

[27] Qinjiang, R.: Resonant frequencies of arbitrary shaped microstrip patch antennas, in Antennas and Propagation Society Int. Symp., Chicago, USA, 1992, 1745–1748.

[28] Yang, X.H.; Shafai, L.: Nodal-based basis function for full wave analysis of microstrip antennas with arbitrary geometries. Electron. Lett., **30** (1994), 830–831.

[29] Omar, A.A.; Chow, Y.L.; Stubbs, M.G.: Contour integral method with fringe complex images for the rapid solution of patch resonators of arbitrary shape. IEEE Trans. Microw. Theory Tech., **43** (1995), 2028–2034.

[30] Okoshi, T.: Planar Circuits for Microwaves and Lightwaves, Springer Series in Electronics and Photonics, New York, 1985.

[31] Sun, Y.; Chow, Y.L.; Fang, D.G.: Irregularly shaped patch as perturbation of regularly shaped patch, in Antennas and Propagation Society Int. Symp., Boston, USA, vol. **1**, 2001, 502–505.

[32] Tiang, J.J.; Islam, M.T.; Misran, N.; Mandeep, J.S.: Circular microstrip slot antenna for dual-frequency RFID application. Prog. Electromagn. Res., **120** (2011), 499–512.

[33] Bilotti, F.; Al'U, A.; Manzini, M.: Design of polygonal patch antennas with a broad-band behavior via a proper perturbation of conventional rectangular radiators, in Antennas and Propagation Society Int. Symp., Columbus, USA, vol. **2**, 2003, 268–271.

[34] Manzini, M.; Andrea, A.; Bilotti, F.; Vegni, L.: Polygonal patch antennas for wireless communications. IEEE Trans. Veh. Tech., **53** (2004), 1434–1440.

[35] Bilotti, F.; Al'U, A.; Vegni, L.: Electromagnetic field solution in conformal structures: theoretical and numerical analysis. Prog. Electromagn. Res., **47** (2004), 1–25.

[36] Sarder, J.E.: Analysis of arbitrary profiles by implementation of integral equation eigenvalue analysis. IEEE J. Quantum Electron., **26** (1990), 2013–2024.

[37] Sarder, J.E.: Integral equation analysis for higher order modes and cutoff frequencies of arbitrary profiles. IEEE J. Quantum Electron., **27** (1991), 976–984.

[38] Pozar, D.M.: Microwave Engineering, J. Wiley & Sons Inc., USA, 2005.

[39] Balanis, C.A.: Advanced Engineering Electromagnetics, J. Wiley & Sons Inc., USA, 1989.

[40] Ansys Ansoft HFSS simulator version 14.0, Ansys Corp., Canonsburg, PA, USA.

https://doi.org/10.1017/S1759078717000368 Published online by Cambridge University Press

Karishma Sharma received her B.Tech. degree in Electronics and Communication Engineering in 2011 from GGSIPU, Delhi, India. She was awarded gold medal and an exemplary performer in her M.Tech., from GGSIPU, Delhi, India in 2013. She is currently pursuing her Ph.D. in the area of Design and Analysis of Microstrip patch antenna from Netaji Subhas Institute of Technology, Delhi University, Delhi, India. Her research interests include antenna design and its analysis, applied electromagnetic theory, metamaterials, digital, and wireless communication.

Dharmendra K. Upadhyay holds Bachelor of Engineering in Electronics and Communication Engineering from Kumaon University, Nainital, India and Master of Technology in Communication and Information Systems from Aligarh Muslim University, Aligarh, UP, India. He obtained his Ph.D. from Uttrakhand Technical University, Dehradun, Uttrakhand, India in 2013. Presently, he is associated with Netaji Subhas Institute of Technology, Delhi, India, as a Professor in the Division of Electronics and Communication Engineering. He has published several papers in various International Journals. He is a life member of ISTE. His research interests include microstrip patch antenna designs, microwave filters, and digital signal processing.

Harish Parthasarathy received the Bachelor's degree in 1990 from the Indian Institute of Technology, Kanpur, India and Ph.D. in 1994 from the Indian Institute of Technology, Delhi, India, both in Electrical Engineering. He is currently working as a Professor at Netaji Subhas Institute of Technology, Delhi University, Delhi, India. He is an eminent academician and a great researcher, and has authored more than 100 research articles in various international journals of repute. His research interests include the areas of electromagnetic theory, antennas, quantum mechanics, circuits and systems, signal processing, and stochastic nonlinear filters.

https://doi.org/10.1017/S1759078717000368 Published online by Cambridge University Press